Estimation of rotation angle and anisotropic scaling rate using pilot signals for watermarking

Rinka Kawano and Masaki Kawamura
* Graduate School of Sciences and Technology for Innovation, Yamaguchi University
E-mail: {rinka1005,m.kawamura}@m.ieice.org Tel: +81-83-933-5701

***Abstract*—We propose a method for simultaneously estimating the rotation angle and anisotropic scaling rates. Conventional watermarking methods are robust against non-geometric attacks. However, these methods need to synchronize to resist geometric attacks. Invariant features, such as SIFT, have been used for the synchronization. In this paper, we focus on pilot signals for estimating geometric attacks. By embedding a grid-shaped pilot signal and detecting its change, individual attacks on the scaling rate and rotation angle can be estimated. However, it has been difficult to estimate combined attacks. Our proposed method for estimating rotation angle and anisotropic scaling rates uses Radon coefficients. A Radon transform is applied to the signal obtained by QIM from a stego image. Periodic strong peaks appear in the coefficients at rotation angles. The period of the peaks is also calculated. From the rotation angle and the period at which the peaks appear, the rotation angle and the anisotropic scaling rates can be estimated. Computational results show that the rotation angle can be successfully estimated with an absolute error below 0.2 degrees. In more than half of the results, the absolute error of the anisotropic scaling rates was almost zero.**

I. Introduction

Unauthorized use of digital content posted on social media has become a problem. Digital watermarking [1] has been focused on as one of the technologies to protect digital content. Digital watermarking is a technique for secretly embedding other information in digital content. The embedded information is called a watermark. An image in which the watermark is embedded is called a stego image. It is possible to manage content and detect unauthorized use by embedding user IDs and other information in distributed images. However, illegal users often alter distributed images by scaling, rotating, cropping, etc. They also compress the images when they are saved. This leads to image degradation. These alterations (attacks) to stego images can cause the watermark to disappear or make it difficult to detect the watermark. Thus, the watermark needs to be robust against various attacks.

There are two main types of attacks on images: non-geometric attacks and geometric attacks. Non-geometric attacks, such as JPEG compression and noise addition, change the pixel values. The watermark is also degraded when a non-geometric attack is applied to an image. As a result, the watermark cannot be extracted. Methods robust against non-geometric attacks include those using error-correcting code [2] and spread spectrum [3], [4]. By applying redundancy to the watermark, these methods can correct errors in degraded watermarks.

In contrast, geometric attacks such as scaling, rotating, cropping, etc. change the position of pixels. It is necessary to detect the embedding position because a geometric attack on an image changes the coordinates at which the watermark is embedded. As a method robust against geometric attacks, some watermarking methods using the SIFT feature [5], [6], [7], [8], have been proposed. By embedding watermarking around multiple SIFT features, it is possible to improve the resistance to geometric attacks. An embedding method that is robust to linear transformations by normalizing images to a universal shape was proposed by P. Dong et al. [9]. However, both the image and the watermark itself can be degraded by the normalization.

Many conventional methods require knowledge on the parameters of inverse transformation or involve computationally expensive processes such as brute force against geometric attacks. As a result, these methods lack sufficient tolerance to unknown geometric attacks. If we could estimate the type and strength of geometric attacks, we could detect the exact location of the watermark, reducing the number of watermarking errors. For this reason, we have focused on the framework of communication channel estimation in order to estimate the type and strength of the attacks [10]. There is a method that uses a signal different from the message, called a pilot signal, for communication channel estimation. When a pilot signal is transmitted, it is degraded by the communication channel, so the degree of degradation can be used to estimate the parameters of the channel. By introducing the pilot signal into the watermarking scheme, pilot signal degradation can be used to estimate the attack parameters.

A watermarking method using a pilot signal was proposed by Su *et al.* [11]. In their method, a pilot signal was embedded to detect the locations of embedding regions around SIFT feature points. The direction of the embedding regions was determined using the gradient of the SIFT features. The watermarks were embedded into the rotated embedding regions. This method is robust with respect to the change in coordinates. However, it is necessary to rotate the regions in the gradient direction during watermark embedding and extraction. Since these processes are also geometric attacks, they degrade the watermark and image quality.

A new approach is needed to estimate the type and intensity of geometric attacks. To estimate attacks from pilot signals, it is necessary to determine the appropriate embedding method and the shape of the signal for each attack. Since there are different types of attacks, it is necessary to generate signals and develop extraction methods for each type. In our previous

work, we developed a method for estimating attacks with the use of a grid-shaped pilot signal. We showed that individual attacks, i.e., scaling and rotation attacks, can be estimated using the pilot signal [12]. The watermark could also be estimated from the estimated scaling rate [13]. However, it is difficult to estimate these combined attacks.

As an example of estimating a simple composite attack, we proposed a method for estimating the rotation angle and scaling rate simultaneously using the Radon transform [10]. The Radon transform is an integral transform that line integrates an image from different angles. When a grid-shaped pilot signal is Radon transformed, strong intensities appear in the Radon coefficients due to line integration at the same angle as the grid. Therefore, by determining the angle at which strong intensities appear in the Radon coefficient, the rotation angle can be estimated. Also, these strong intensities appear with the same period as the grid interval. Thus, the scaling rate can be estimated by detecting this interval and comparing it with the original grid interval. However, this method is only effective for attack detection when the horizontal and vertical scaling rates are equal. When anisotropic scaling is performed on an image, the orthogonality of the grid lines is lost, so the anisotropic scaling rate and the rotation angle cannot be estimated simultaneously. In this paper, we propose a method for simultaneously estimating the rotation angle and the anisotropic scaling rate. We theoretically derive equations for estimating these attack parameters from Radon coefficients. We also validate these equations with computer simulations.

This paper is organized as follows. Section II outlines the method for estimating the rotation angle and anisotropic scaling rate using the pilot signal. Theoretical equations for the rotation angle and the grid interval estimated from the Radon coefficient are derived. Section III describes the results of computer simulations to verify the theoretical equations, and Sec. IV concludes our study.

II. Geometric transformations and Radon transform

In the proposed method, a grid-shaped pilot signal is embedded in the original image. By detecting changes in the signal, geometric attacks such as rotation and anisotropic scaling are estimated. From the Radon coefficients obtained by Radon transform of the pilot signal obtained from the attacked image, the rotation angle and the scaling rate are estimated. The estimation procedure is carried out as follows. (i) The pilot signal is extracted from the attacked image. (ii) The pilot signal is transformed by Radon transform to obtain the detection angle and the detection interval. (iii) The rotation angle and scaling rate are estimated using both the detection angle and the detection interval.

The assumed attack combinations are rotation and anisotropic scaling. Let T_θ be the rotation matrix when the rotation angle is θ. Let $T_S = \mathrm{diag}(S_x, S_y)$ be the scaling matrix when the scaling rate on the x-axis is S_x and the scaling rate on the y-axis is S_y. The transformation matrix when the image is scaled and then rotated is given by

$$T_\theta T_S = \begin{pmatrix} S_x \cos\theta & -S_y \sin\theta \\ S_x \sin\theta & S_y \cos\theta \end{pmatrix}. \quad (1)$$

The transformation matrix when the image is rotated and then scaled is given by

$$T_S T_\theta = \begin{pmatrix} S_x \cos\theta & -S_x \sin\theta \\ S_y \sin\theta & S_y \cos\theta \end{pmatrix}. \quad (2)$$

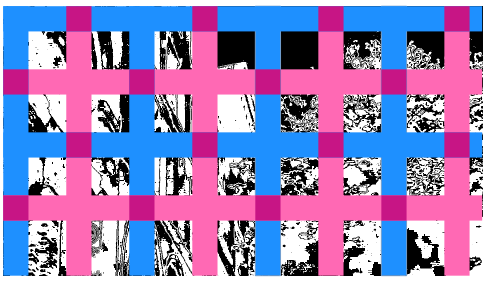

Fig. 1. Pilot signal instead of watermark. Note that pilot signal $p \in 0, 1$ is embedded in pixel value $U(i, j)$.

A. Pilot signal

The image is decomposed into a YUV color space. A pilot signal is embedded into the U-component of the image using QIM [14]. The shape of the pilot signal is a grid as shown in Figure 1 and consists of two directional lines, one at an angle of $\psi_h = 0$ to the x-axis and the other at an angle of $\psi_v = \pi/2$. The interval between the lines of the same color is set to $\gamma = 100$ pixels. The width of the lines is set to 5 pixels. The values on the lines take on two values. The values 0 and 1 are embedded in the pilot signals of the blue and red lines, respectively. The purple area, which is the intersection of the two types of lines, is embedded with alternately equal percentages of 1 and 0. No changes are applied to the regions other than the pilot signal. This means that during detection, image-specific components are detected in the regions where no pilot signal is embedded.

B. Extraction of pilot signals and Radon transformation

First, the stego image is decomposed into the YUV color space. From the U-component image $U'(x, y)$, a binary signal is obtained with QIM [14]. This signal is called the extracted signal $\hat{p}(x, y)$. Applying the Radon transform to the extracted signal $\hat{p}(x, y)$, the slope of lines in the signal can be detected as a feature. Let us consider the case where only rotation is applied to the image. Let ϕ_1 and ϕ_2 be the detection angles obtained from the Radon coefficients when the image is rotated by the angle $0 \leq \theta < \pi/2$. Figure 2 shows a schematic diagram of the Radon coefficients of the pilot signal extracted from the rotated image. The vertical axis is the projection position, and the horizontal axis is the projection angle. When a grid-shaped pilot signal, consisting of straight lines in two orthogonal directions, is Radon-transformed, strong intensities appear at two angles, ϕ_1 and ϕ_2 ($\phi_1 < \phi_2$), as shown in the figure.

The method used to estimate the detection angle and detection interval from the Radon coefficients is an adapted version of the

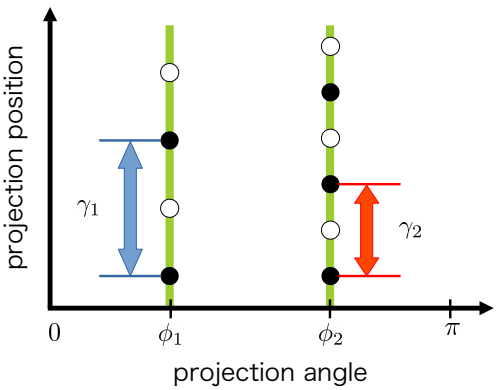

Fig. 2. Schematic diagram of Radon coefficients

method in our previous study [10]. Here, we briefly describe how to detect strong intensities from Radon coefficients and calculate detection intervals. Strong intensities appear at equal intervals at detection angles ϕ_1 and ϕ_2. From the variance of the Radon coefficients for each projection angle, we can see that the variance is large at the projection angles ϕ_1 and ϕ_2. Therefore, the detection angles ϕ_1 and ϕ_2 can be obtained by detecting the peaks from the variance of the Radon coefficient at each projection angle. At angles ϕ_1 and ϕ_2, there are strong periodic intensities in the Radon coefficients. Each interval is called a detection interval, denoted by γ_1 and γ_2. The Radon coefficients contain not only the pilot signal but also components of the original image. Therefore, it is difficult to determine the detection interval automatically. After calculating the autocorrelation of the Radon coefficients, the detection interval is obtained by using DFT on the autocorrelation coefficients. The grid interval of the pilot signal coincides with the detection interval only in the case of rotation. The relationship between the detection angles ϕ_1, ϕ_2 and the rotation angle θ is derived theoretically in this section.

In the Radon transform, the projection plane is rotated clockwise from the y-axis in order to detect components perpendicular to the projection plane. This means that the projection plane of the Radon transform is shifted by $\pi/2$. In contrast, the geometric transform rotates counterclockwise. Note that due to the difference in the direction of rotation between the geometric and Radon transform, the angle of rotation on the Radon coefficients is represented as $-\theta$. Let ϕ_h and ϕ_v be the angles after θ rotation of the horizontal component $\psi_h = 0$ and the vertical component $\psi_v = \pi/2$ of the pilot signal. They are given by

$$\phi_h = \frac{\pi}{2} - \theta + \psi_h = \frac{\pi}{2} - \theta \bmod \pi, \tag{3}$$

$$\phi_v = \pi - \theta + \psi_v = \frac{\pi}{2} - \theta \bmod \pi. \tag{4}$$

Thus, the estimated rotation angle $\hat{\theta}$ is obtained by

$$\hat{\theta} = \frac{1}{2}\left(\phi_h + \phi_v - \frac{3\pi}{2}\right). \tag{5}$$

Since the pilot signal is rotationally symmetric, rotations by whole integer multiples of $\pi/2$ are indistinguishable.

C. Combined attack of rotation and anisotropic scaling

As expressed in (1) and (2), when an image is attacked by rotation and anisotropic scaling, the results depend on the order of the attacks. When the image is rotated after anisotropic scaling, the rotation angle $\hat{\theta}$ is given by (5) since equations (3) and (4) hold. The scaling rates can be estimated by using the detection intervals γ_1 and γ_2 on the detection angles ϕ_1 and ϕ_2. When the horizontal component ϕ_h of the pilot signal is detected as the detection angle ϕ_1, the detection interval γ_1 on ϕ_1 corresponds to the grid interval of the vertical component ψ_v. Therefore, when the original grid interval is γ, the estimated scaling rates $\hat{S}_x$ and $\hat{S}_y$ are calculated by

$$\hat{S}_x = \frac{\gamma_2}{\gamma}, \ \hat{S}_y = \frac{\gamma_1}{\gamma}. \tag{6}$$

On the other hand, when anisotropic scaling is performed after image rotation, the orthogonality of the grid lines is broken, and Eqs. (3) and (4) do not hold. In this paper, we derive an estimation method for this case. Let us consider the case where the rotation angle is between 0 and $\pi/2$. In this case, the detection angles for the horizontal component ψ_h and the vertical component ψ_v are $\phi_h < \phi_v$, so $\phi_h = \phi_1$ and $\phi_v = \phi_2$. The derivation is described in Appendix A. From (25), the tangent of the estimated rotation angle $\hat{\theta}$ is given by

$$\tan\hat{\theta} = \mathrm{sgn}\left(\frac{1}{\tan\phi_1}\right)\sqrt{-\frac{\tan\phi_2}{\tan\phi_1}}, \tag{7}$$

where $\mathrm{sgn}(x)$ is the sign function. The actual angle of rotation θ is between 0 and 2π. Therefore, there are two possible solutions to (7). Also, the estimated scaling rates $\hat{S}_x$ and $\hat{S}_y$ are given by

$$\hat{S}_x = \sqrt{\frac{\gamma_1\gamma_2 \tan\phi_1 \tan\hat{\theta}}{\gamma^2 \sin|\phi_2 - \phi_1|}}, \tag{8}$$

$$\hat{S}_y = \sqrt{\frac{\gamma_1\gamma_2}{\gamma^2 \tan\phi_1 \tan\hat{\theta} \sin|\phi_2 - \phi_1|}}. \tag{9}$$

D. In case of right angles

If the detection angle ϕ_1 is 0 or π, then $\tan\phi_1 = 0$. Therefore, (7) is not computable. Similarly, $\tan\hat{\theta}$ in (9) includes $\tan\phi_2$. Therefore, if the detection angle ϕ_2 is 0 or π, then $\tan\phi_2 = 0$. Therefore, (9) is not computable. In this paper, rotation and anisotropic scaling are applied to the image once each. As a result, the detection angle ϕ_1 or ϕ_2 becomes zero only if the rotation angle satisfies $\theta = n\pi/2, n = 0, 1, 2, 3$. Therefore, when the detection angle ϕ_1 or ϕ_2 is 0 or π, the estimated rotation angle and the estimated scaling rates are obtained by (5) as in the case of rotation after anisotropic scaling of the image. The estimated scaling rates are given by (6).

III. COMPUTER SIMULATION

We derived equations to estimate the attack parameters by detecting the pilot signal from the Radon coefficients. This section demonstrates that our theoretical equations are correct.

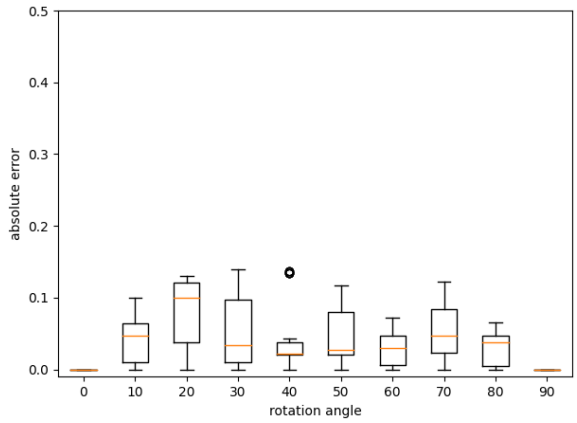

Fig. 3. Absolute error $|\hat{\theta} - \theta|$ for each angle: Orange line represents medians of results.

Specifically, we evaluated our method for estimating the rotation angle and the anisotropic scaling rates with absolute error when the stego image was rotated and then anisotropically scaled.

A. Experimental conditions

The pilot signal was embedded in the U-component of six IHC standard images of 4608×3456 pixels [15]. We considered attacks in which the stego images were rotated, anisotropically scaled, and then cropped. The angles of rotation were set to $0, 10, 20, \cdots, 90$ degrees. In addition, the scaling rate for the x-axis S_x was set to 1, and the scaling rates for the y-axis were assumed to be $S_y = 0.5, 0.6, \cdots, 1.5$. Since the Radon transform is performed on a square surface, the stego images were cropped to a size of 1080×1080 pixels from the center of the image after the geometric transformation.

B. Experimental results

First, we evaluated the estimated rotation angle $\hat{\theta}$ in terms of the absolute error $|\hat{\theta} - \theta|$. Since our pilot signal is grid-shaped, four candidates are detected as estimated rotation angles. These are indistinguishable. Therefore, the angle closest to the true rotation angle was treated as the estimated rotation angle. There were $11 \times 6 = 66$ results since there were 11 different scaling rates in the y-axis direction. Figure 3 shows their box-and-whisker plots. The horizontal axis is the rotation angle θ. The vertical axis is the absolute error $|\hat{\theta} - \theta|$. The orange line represents the medians of the results. All rotation angles were successfully estimated with an absolute error of less than 0.2 degrees.

Next, the estimated scaling rates were evaluated. The absolute errors of the estimated scaling rates $\hat{S}_x$ and $\hat{S}_y$ are shown in Figure 4 as box-and-whisker plots. The horizontal axis is the scaling rate S_y. Now remember that we set $S_x = 1.0$. The vertical axis represents the absolute errors of (a) the estimated scaling rates $\hat{S}_x$ and (b) $\hat{S}_y$. The orange line represents their medians. For all scaling rates, the medians were close to zero. However, we found that many results had a large absolute error for scaling rates greater than 1.0.

We considered the reason why the estimation errors are more frequent when the scaling rate is large. From our previous study [10], we know that the larger the scaling rate, the more likely it is that the grid interval γ_1 and γ_2 will fail detection. This is due to the fact that when a scaled image is cropped to a given size, the larger the scaling rate, the fewer the number of grid lines within the cropped image. In addition, if the components of the original image are not smooth, the components may cause the peak to not be detected, resulting in incorrect period estimation. In summary, the reason why the absolute error of the scaling rate was large, while the estimated rotation angle was calculated accurately, is due to the inaccurate detection of the grid intervals γ_1 and γ_2.

IV. Conclusion

Blind watermarking methods need to be robust against geometric attacks. Methods with redundant watermark embedding are ineffective against geometric attacks. Therefore, methods that assume geometric attacks by using SIFT feature points and the polar coordinate system have been proposed. We proposed a grid-shaped pilot signal for estimating geometric attacks. So far, we have been successful in estimating a single attack, either a rotational attack or an isotropic scaling attack [10]. The angle and interval of the grid can be obtained by applying the Radon transform to the pilot signal extracted from the image.

In this paper, we proposed a method for estimating both the rotation angle and the anisotropic scaling rates from images attacked by a combined rotation attack and anisotropic scaling attack. We theoretically derived the estimated rotation angle and the estimated scaling rates from the Radon coefficients and the geometric transformation matrix. Using both the detection angles and the detection intervals obtained from the Radon coefficients, the estimated rotation angle and the estimated scaling rates can be calculated. To demonstrate the correctness of the estimators obtained from our theory, we validated them in computer simulations. In particular, we verified the accuracy of the estimators for the case of anisotropic scaling after rotating stego images. As a result, it was possible to estimate the rotation angle with an absolute error of less than 0.2 degrees. The median of the estimates was zero for the estimation of anisotropic scaling. That is, the absolute error was zero for more than half of the results. In particular, the estimation was almost accurate when the scaling rate was less than 1. In contrast, when the scaling rate was greater than 1, the number of cases with large absolute errors increased. This is due to inaccuracies in the estimates of the detection intervals γ_1 and γ_2.

The proposed method could estimate the combined rotation and scaling attacks. However, the scaling rate needs to be estimated more accurately. It is necessary to improve the detection of peaks from the Radon coefficients to accurately detect the detection intervals γ_1 and γ_2. Improving the detection algorithm and estimating general geometric transformations including shear is our future work.

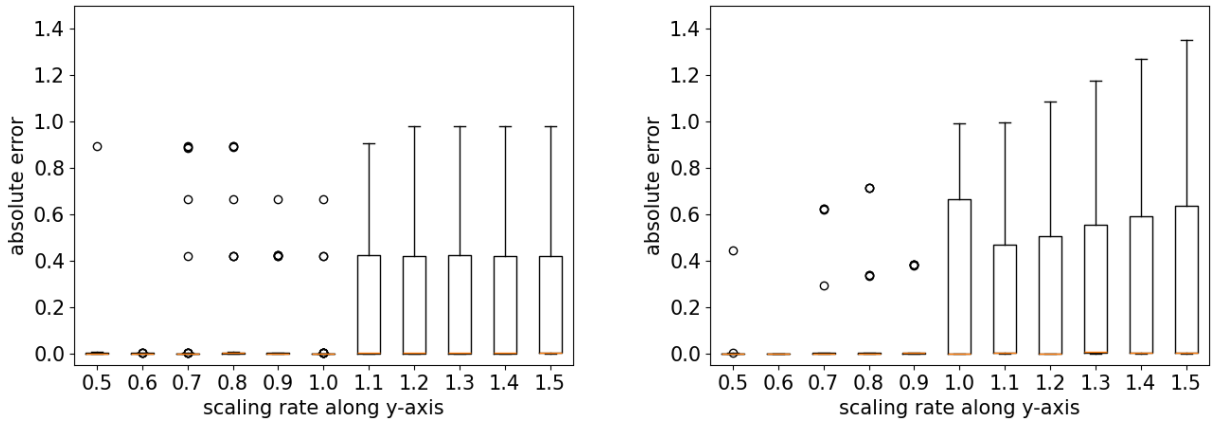

(a) Scaling rate in x-axis direction, $\hat{S}_x$ (b) Scaling rate in y-axis direction, $\hat{S}_y$

Fig. 4. Absolute error of estimated scaling rates

V. Acknowledgment

This work was supported by JSPS KAKENHI Grant Number JP20K11973 and JP24K15106, the Telecommunications Advancement Foundation, the Yamaguchi University Fund, and the Cooperative Research Project Program, R04/B09 Research on Multifunctional Multimedia Production, of the RIEC, Tohoku University. A part of the computations were performed using the supercomputer facilities at the Research Institute for Information Technology, Kyushu University.

References

[1] F. A. Petitcolas, R. J. Anderson, M. G. Kuhn, "Information hiding-a survey," Proceedings of the IEEE, vol. 87, no. 7, pp. 1062–1078, 1999
[2] H. Kang, K. Iwamura, "Watermarking based on the difference of discrete cosine transform coefficients and an error-correcting code," Proc. of IWIHC, pp. 9–17, 2014
[3] I. J. Cox, J. Kilian, F. T. Leighton and T. Shamoon, "Secure spread spectrum watermarking for multimedia," in IEEE Transactions on Image Processing, vol. 6, no. 12, pp. 1673–1687, 1997
[4] J. J.K.O. Ruanaidh, T. Pun, "Rotation, scale and translation invariant spread spectrum digital image watermarking," Signal Process., vol. 66, Issue 3, pp. 303–317, 1998
[5] D. G. Lowe, "Distinctive image features from scale-invariant keypoints," International J. Compute Vision, vol. 60, no. 2, pp. 91–110, 2004
[6] M. Hayashi, M. Kawamura, "Improved SIFT feature-based watermarking method for IHC ver. 5," Proc. of APSIPA ASC 2018, pp. 1536–1543, 2018
[7] V. Solachidis, I. Pitas, "Circularly symmetric watermark embedding in 2-D DFT domain," IEEE Trans Image Process, vol. 10, no. 11, pp. 1741–1752, 2001
[8] J. S. Seo, C. D. Yoo, "Localized image watermarking based on feature points of scale-space representation," Pattern Recognition, vol. 37, Issue 7, pp. 1365–1375, 2004
[9] P. Dong, J. G. Brankov, N. P. Galatsanos, Y. Yang and F. Davoine, "Digital watermarking robust to geometric distortions," in IEEE Trans. on Image Processing, vol. 14, no. 12, pp. 2140–2150, 2005
[10] R. Kawano, M. Kawamura, "Estimation of scaling rate and rotation angle using pilot signal for image watermarking," IEICE Technical Report, vol. 123, no. 407, pp. 28–33, 2024
[11] P. C. Su, Y. C. Chang and C. Y. Wu, "Geometrically resilient digital image watermarking by using interest point extraction and extended pilot signals," IEEE Trans. Inf. Forensics Secur., vol. 8, no. 12, pp. 1897–1908, 2013
[12] R. Kawano, M. Kawamura, "Detection of periodic pilot signal in image watermarking," APSIPA ASC 2021, SS-IVM-1.6, pp. 1647–1652, 2021
[13] R. Kawano, M. Kawamura, "Watermarking method with scaling rate estimation using pilot signal," IEICE Trans. Inf. & Syst., vol. E107-D, no. 9, 2024
[14] B. Chen, G. W. Wornell, "Quantization index modulation: a class of provably good methods for digital watermarking and information embedding," IEEE Trans. Inf. Theory, vol. 47, no. 4, pp. 1423–1443, 2001
[15] Information Hiding and its Criteria for evaluation, https://www.ieice.org/iss/emm/ihc/en/image/image.php (20th February, 2023 access)

Appendix

A. Estimation of rotation angle

We will consider the case where the rotation angle θ is in $0 \leq \theta < \pi/2$. The detection angles obtained from the Radon coefficients are ϕ_1 and ϕ_2 ($\phi_1 < \phi_2$). The projective plane of the Radon transformation is shifted by $\pi/2$. The direction of rotation is opposite that of the rotation transformation. Let $A'(x_a, y_a)$, $B'(x_b, y_b)$, and $C'(x_c, y_c)$ be points $A(\gamma, 0)$ on the horizontal component ϕ_h of the pilot signal, $B(0, \gamma)$ on the vertical component ϕ_v and $C(\gamma, \gamma)$ after the transformation. Let α be the angle between the x-axis and line OA'. Let β be the angle between the x-axis and line OB'.

Figure 5 shows these angles α, β, ϕ_1, and ϕ_2. The angles α and β are represented by

$$\alpha = \frac{\pi}{2} - \phi_1,\ \beta = \frac{3\pi}{2} - \phi_2. \tag{10}$$

The tangent of these angles is therefore given by

$$\tan\alpha = \frac{1}{\tan\phi_1},\ \ \tan\beta = -\frac{1}{\tan\phi_2}. \tag{11}$$

Therefore, the angle $\angle A'OB' = |\beta - \alpha|$ between line OA' and line OB' is given by

$$|\beta - \alpha| = |\pi + \phi_1 - \phi_2|. \tag{12}$$

Point A' projected from point A is given by

$$\begin{pmatrix} x_a \\ y_a \end{pmatrix} = T_\theta T_S \begin{pmatrix} \gamma \\ 0 \end{pmatrix} = \begin{pmatrix} \gamma S_x \cos\theta \\ \gamma S_y \sin\theta \end{pmatrix}. \tag{13}$$

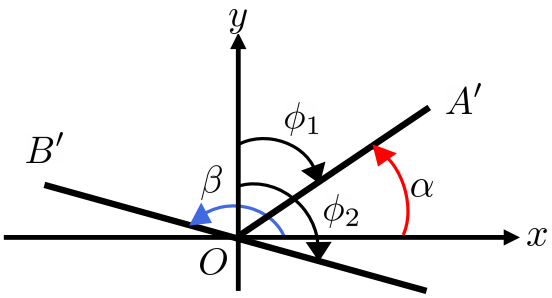

Fig. 5. Relationship between angles α, β, ϕ_1, and ϕ_2.

Therefore, the tangent of the slope of line OA', $\tan\alpha$, is given by

$$\tan\alpha = \frac{S_y}{S_x}\tan\theta. \tag{14}$$

Similarly, point B' projected from point B is given by

$$\begin{pmatrix} x_b \\ y_b \end{pmatrix} = T_\theta T_S \begin{pmatrix} 0 \\ \gamma \end{pmatrix} = \begin{pmatrix} -\gamma S_x \gamma \sin\theta \\ \gamma S_y \gamma \cos\theta \end{pmatrix}. \tag{15}$$

Therefore, the tangent of the slope of line OB', $\tan\beta$, is given by

$$\tan\beta = \frac{S_y}{S_x}\left(-\frac{1}{\tan\theta}\right). \tag{16}$$

From (14) and (16), we obtain

$$-\frac{\tan\alpha}{\tan\beta} = -\frac{\tan\phi_2}{\tan\phi_1} = \tan^2\theta. \tag{17}$$

The signs of the tangents of the two detection angles ϕ_1 and ϕ_2 are always different, even if the orthogonal grids are rotated and scaled anisotropically. Therefore, the sign of tangent $\tan\hat{\theta}$ of the estimated rotation angle and that of tangent $\tan\alpha$ of the detection angle are always the same. Therefore, from (11), the tangent of the estimated rotation angle $\hat{\theta}$ is given by

$$\tan\hat{\theta} = \mathrm{sgn}\left(\frac{1}{\tan\phi_1}\right)\sqrt{-\frac{\tan\phi_2}{\tan\phi_1}}, \tag{18}$$

where $\mathrm{sgn}(x)$ is the sign function.

B. Estimation of scaling rates

Let us first consider the area Q of the quadrilateral $OA'C'B'$ to find the scaling rates. Since the quadrangle $OA'C'B'$ is a parallelogram, the area of the parallelogram is expressed as

$$Q = |OA'||OB'|\sin|\beta-\alpha|. \tag{19}$$

The parallelogram $OA'C'B'$ and the grid intervals γ_1, γ_2 are shown in Figure 6. The distance between line OA' and line $B'C'$ is represented by the grid interval γ_1, and the distance between line OB' and line $A'C'$ is represented by the grid interval γ_2. The lengths of edges $|OA'|$ and $|OB'|$ are therefore given by

$$|OA'| = \frac{\gamma_2}{\sin|\beta-\alpha|},\ |OB'| = \frac{\gamma_2}{\sin|\beta-\alpha|}. \tag{20}$$

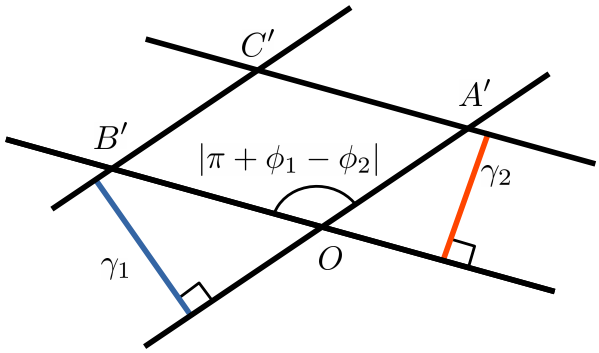

Fig. 6. Relationship between quadrilateral $OA'C'B'$ and grid intervals γ_1, γ_2.

From (19), the area Q is expressed as

$$Q = \frac{\gamma_1\gamma_2}{\sin|\beta-\alpha|}. \tag{21}$$

Next, we calculate the area Q of the parallelogram in a different way, focusing on (13) and (15). From (12), $\sin|\beta-\alpha|$ can be expanded as

$$\begin{aligned}
\sin|\beta-\alpha| &= \sin|\pi+\phi_1-\phi_2| && (22)\\
&= \sin|\phi_2-\phi_1| && (23)\\
&= \sin\phi_2\cos\phi_1 - \cos\phi_2\sin\phi_1 && (24)\\
&= \frac{y_b}{|OB'|}\cdot\frac{x_a}{|OA'|} - \frac{x_b}{|OB'|}\cdot\frac{y_a}{|OA'|} && (25)\\
&= \frac{\gamma^2 S_x S_y}{|OA'||OB'|}. && (26)
\end{aligned}$$

Therefore, from (19), the area Q is given as

$$Q = |OA'||OB'|\cdot\frac{\gamma^2 S_x S_y}{|OA'||OB'|} = S_x S_y \gamma^2. \tag{27}$$

This equation states that the area γ^2 before the transformation is equal to the area multiplied by S_xS_y after the transformation at the anisotropic scaling rates.

Finally, from (21) and (27) we obtain

$$S_x S_y = \frac{\gamma_1\gamma_2}{\gamma^2\sin|\phi_2-\phi_1|}. \tag{28}$$

Using (11) and (14), we obtain

$$S_y = \frac{S_x}{\tan\phi_1\tan\theta}. \tag{29}$$

Substituting this into (28), the estimated scaling rate $\hat{S}_x$ is given by

$$\hat{S}_x = \sqrt{\frac{\gamma_1\gamma_2\tan\phi_1\tan\hat{\theta}}{\gamma^2\sin|\phi_2-\phi_1|}}. \tag{30}$$

Similarly, the estimated scaling rate $\hat{S}_y$ is given by

$$\hat{S}_y = \sqrt{\frac{\gamma_1\gamma_2}{\gamma^2\tan\phi_1\tan\hat{\theta}\sin|\phi_2-\phi_1|}}. \tag{31}$$